Conductive UV-Cured acrylic inks for resistor fabrication: models for their electrical properties

# Conductive UV-Cured Acrylic Inks for Resistor Fabrication: Models for their Electrical Properties

A. Chiolerio,* L. Vescovo, M. Sangermano

We report the preparation of acrylic inks for specific electrical applications, such as resistors, based on a UV-cured resin (PEGDA), where an in situ synthesis of silver nanoparticles is performed. The conversion, gel content and morphology of the nanoparticles, with a specific interest about the size distribution and electrical conductivity at room temperature, are considered. Aging and electromigration are evaluated to confirm the stability of the samples. A correlation between the morphological properties and the electrical ones is given, in particular developing the universal percolation theory and an extension of the Vegard law for composites. Interesting conclusions are drawn based on the application of the models.

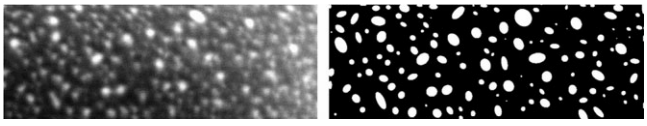

## Introduction

Information technology has become an important part of our lives, requiring a wide variety of electronic components and ever-larger data storage capabilities and memory devices. Organic and polymeric materials are promising candidates for these applications. Their attractiveness include good processability, miniaturized dimensions, good mechanical strength and flexibility.[1] Organic and polymer transistors have been proposed for applications such as display switches and display drivers,[2] radiofrequency identification tags (RFID) and sensors.[3–5]

As alternatives to the more elaborate processes of vacuum evaporation and deposition, solution processes – including spin-coating, spray coating, dip coating, roller coating and ink-jet printing – can be used to deposit polymers on a variety of substrates.[1] For these applications, a very low viscosity should be maintained in the polymer precursor and fast polymerization needs to be performed soon after the deposition.

In order to obtain conductive inks for mass production of electronic components, conductive nanoparticles (NPs) have to be dispersed in a polymeric material to allow the realization of a conductive network (referring to the percolation theory, the so-called "infinite cluster")[6] to ensure the required electrical properties, leading to the formation of a dissipative element. Nevertheless the dispersion of a large amount of metal NPs into a curable formulation could increase the viscosity too much, such that solution processes can no longer be employed.

As an interesting and elegant alternative, Yagci and Sangermano proposed an in situ synthesis of silver-epoxy nanocomposites, which was achieved by simultaneous photoinduced electron transfer and cationic polymerization processes.[7,8] A silver hexafluoroantimonate salt was dissolved into an epoxy resin together with a radical photoinitiator and the formulations were UV irradiated. Stable silver NPs were formed through the oxidation of radicals in the polymerizing medium, together with a cross-linked network due to the carbocations formed from the radicals, which are able to start cationic ring-opening

A. Chiolerio
Physics Department, Politecnico di Torino, Corso Duca degli Abruzzi 24, IT-10129, Torino, Italy
E-mail: alessandro.chiolerio@polito.it
L. Vescovo, M. Sangermano
Materials Science and Chemical Engineering Department, Politecnico di Torino, Corso Duca degli Abruzzi 24, IT-10129, Torino, Italy

polymerization of epoxy monomers. The silver precursor did not modify the viscosity of the resin.

The same photoreduction process can be used for an acrylic resin, where the radical photoinitiator can still form NPs as well as generating reactive species for crosslinking polymerization. A similar process was again proposed by Yagci and Sangermano, who reported the conditions for an in situ synthesis of gold-crosslinked poly(ethylene glycol) nanocomposites by photoinduced electron transfer and free radical polymerization processes.[9,10]

The use of the UV curing process seems to be very interesting because it is obtained at room temperature, allowing the ink to be polymerized even on thermally sensitive substrates, such as paper. Furthermore, this manufacturing process requires a very short process time.[11,12]

Taking into account the in situ process developed in the literature, in this paper an acrylic conductive ink has been developed following a bottom-up approach in which conductive silver NPs are generated in situ during the UV-induced polymerization process. The ink curing conditions have been investigated by real-time Fourier-transform infrared (FT-IR) spectroscopy. The thermal, morphological and electrical properties of the obtained materials were evaluated after curing.

## Experimental Part

### Materials

Acrylic resin, poly(ethylene glycol diacrylate) (PEGDA, $\overline{M}_w \approx 740\,g \cdot mol^{-1}$, $d = 1.12\,g \cdot cm^{-3}$; Ebecryl 11 Cytec, Belgium), silver hexafluoroantimonate ($AgSbF_6$; Aldrich), and the radical photoinitiator, 1-[4-(2-hydroxyethoxy)phenyl]-2-hydroxy-2-methyl-1-propan-1-one (Irgacure 2959, Ciba) were used as received.

### Sample Preparation

The silver precursor was dissolved in PEGDA at concentrations ranging between 5 and 40 wt.-% and a radical photoinitiator was added (2 wt.-%). The formulations were coated onto glass substrates using a wire-wound applicator, then the films were exposed to UV light (medium pressure mercury lamp, Helios Italquartz, Milano) under nitrogen, with a light intensity on the surface of the sample of about 30 $mW \cdot cm^{-2}$ (measured with EIT photometer). Cured tack-free films of about 100 μm were obtained.

### UV-Curing Process and Sample Characterization

Photopolymerization kinetics were determined by real-time FT-IR spectroscopy, employing a Thermo-Nicolet 5700. The formulations were coated onto a silicon wafer with a thickness of 50 μm. The sample was exposed simultaneously to the UV beam, inducing the polymerization, and to the IR beam, analyzing in situ the extent of reaction. Because the IR absorbance is proportional to the monomer concentration, conversion versus irradiation time profiles could be obtained. Acrylic double bond conversion was followed by monitoring the decrease in the absorbance due to C=C groups in the region centered at 1 635 $cm^{-1}$. A medium-pressure mercury lamp equipped with an optical guide (Hamamatsu LC8) was used to induce photopolymerization (light intensity on the surface of the sample of about 30 $mW \cdot cm^{-2}$).

The gel content of the cured films was determined by measuring the weight loss after 24 h extraction with chloroform at room temperature, according to the standard test method ASTM D2765-84.

DSC measurements were performed using a Mettler DSC 30 (Switzerland) apparatus, equipped with a low temperature probe (heating rate: $20\,K \cdot min^{-1}$).

TGA analyses were performed using a TA instrument in the range 303 to 973 K, with a heating temperature of $10\,K \cdot min^{-1}$ in air.

The morphology of the obtained materials was investigated by means of field-emission scanning-electron microscopy (FESEM; Supra 40 Zeiss instrument). The fracture surfaces of a transverse section of the cured coatings were observed with the in-lens detector. This detector is an ideal tool to investigate polymeric materials thanks to its high detection efficiency at very low acceleration voltages and the almost pure detection of SE electrons. The detector is placed above the objective lens and detects directly the beam path. The lower the energy of the primary electrons, the smaller the interaction volume and the penetration depth of the electrons. The smaller penetration depth of the electrons, the higher the share of SE generated in the upper layers of the specimen, which contribute to the image contrast and resolution. This detector allows to collect images at very low acceleration voltages (1.5–5 kV) with a minimization and compensation of the effects due to the accumulation of local charges on the surface of non-conductive materials, that otherwise can significantly deteriorate imaging quality.

Ag NP images were further processed starting from the transverse sections in order to extract detailed information relative to their size distribution, eccentricity distribution, branching behavior and distance distribution. This task was accomplished using the Matlab® environment and the Image Processing Toolbox 5.4, developing a specific code working on gray scale 2-bit-valued images obtained from filtered portions of the FESEM analysis. The procedure features an automatic particle recognition tool that outputs the number of identified grains or NPs ($n$) and a synthetic reconstruction of the image. Here the grains are substituted by a pattern of ellipsoids, whose centers coincide with the surface centers of mass and whose surface first momenta coincide with those of the particles (see Figure 1). Those ellipsoids give the eccentricity ($E$) distribution; the limit for $E \rightarrow 0$ is achieved by a nanowire. A corresponding population of circles whose centers coincide with the particle surface centers of mass and whose areas coincide with the areas of the particles is also generated, allowing the extraction of an equivalent diameter (ED) distribution. A branching factor (BF) distribution is also produced, considering that a branched particle is such that its area lies predominantly outside the area of its equivalent circle, having $BF < 1$; the limit for $BF \rightarrow 0$ is achieved by a nanowire or a dendritic structure. Finally, the

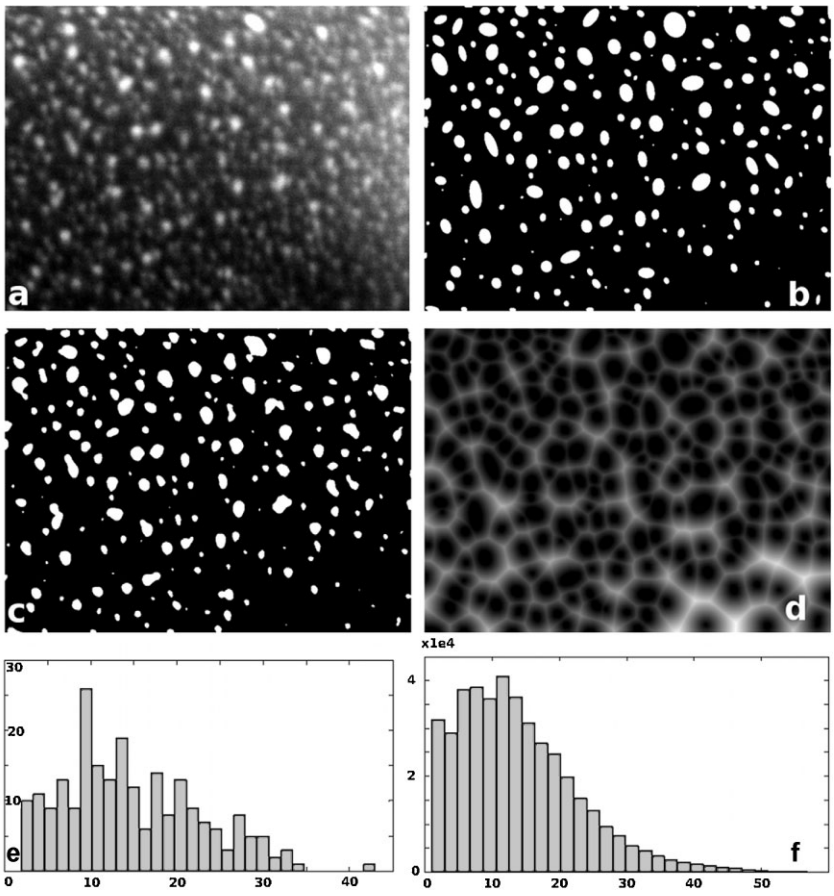


*Figure 1.* Particle recognition and statistical distribution extraction: cured film section containing 10 wt.-% of silver precursor. (a) Raw image (580 × 435 nm at a magnification of 100 000 ×); (b) synthetic pattern of elliptical and circular NPs generated by the numerical algorithm; (c) 2-bit conversion of raw image; (d) Euclidean distance matrix generated by the algorithm from (c); (e) equivalent diameter distribution, output corresponding to the pattern in (b); (f) distance distribution, output corresponding to the pattern in (d).

Euclidean distance (*D*) between pixels belonging to grains is also computed, the relative map generated and the corresponding distribution extracted.

Electrical properties of the cured films were tested with a particular setup, featuring a four-point probe geometry obtained by shadow masking and high vacuum thermal evaporation of Ti (20 nm, adhesion promoter)/Au (200 nm, conduction layer) over the glass and below the nanocomposite. The cured resin was in electrical contact with the underlying electrodes; since the measured resistance was quite high, only two electrodes were used in the samples here compared. Different electrode layouts were also tested, comprehensive of Cu leads and top-lead architectures, but the former proved to be the best and most reliable system. Standard *I/V* measurements were done at room temperature, letting the sample relax with a repetition of non-consecutive measures; resistivity was determined measuring the sample size and the slope of the linear fit of the mean between three measures performed over the domain [−50, +50] V.

## Results and Discussion

### Curing

Recently, it was shown that simultaneous photoinduced electron transfer and cationic polymerization processes exhibited high potential as a novel route to prepare silver epoxy nanocomposites.[9] The emergence of this approach led to develop gold-acrylic based polymer nanocomposites using free radical mode in the process.[10] In this study, we report simultaneous UV-induced radical polymerization of a typical acrylic resin (PEGDA) and silver NP formation by the reduction of $AgSbF_6$ in the presence of a suitable photoinitiator; the UV generated radicals can start the polyaddition reaction of the acrylic resin, and at the same time, they are capable of reducing $Ag^+$ to $Ag^0$ (see Scheme 1). Thus, silver NPs are formed in situ during the polymer network formation, leading to a dissipative nanocomposite. The aim of the work is the exploration of the percolation threshold in order to obtain acrylic conductive UV-curable inks.

FT-IR spectroscopy studies revealed that polymerization proceeded quite rapidly and an almost complete acrylic double bond conversion was achieved within less than one minute of UV irradiation. In Figure 2 we report the real-time FT-IR spectra of the pristine acrylic resin and in the presence of increasing amount of silver precursor. The curves showed a quite high reactivity of the acrylic resin which reaches a conversion of about 50% after a few seconds of irradiation. The presence of the silver precursor did not influence significantly the rate of curing and the final acrylic double bond conversion.

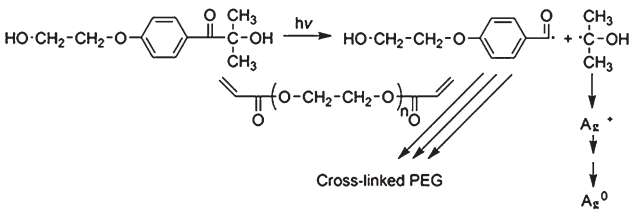


*Scheme 1.* Mechanism of simultaneous UV-induced radical polymerization of a typical acrylic resin (PEGDA) and silver NP formation by the reduction of $AgSbF_6$ in the presence of a suitable photoinitiator.

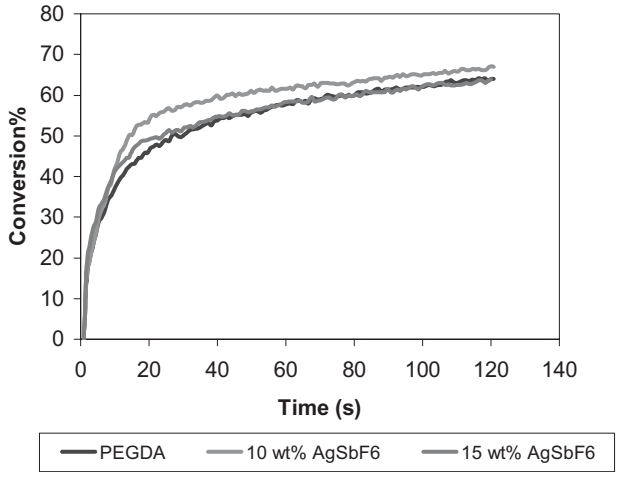


*Figure 2.* Real-time FT-IR spectroscopy conversion curves as a function of irradiation time for the pristine PEGDA resin and in the presence of increasing content of silver precursor.

Nevertheless, these curves were recorded in air, which can inhibit the radical polymerization process with a lower acrylic double bond conversion. For this reason a final acrylic double bond conversion was evaluated by FT-IR analysis: the FT-IR spectra before and after 30 s of UV curing in nitrogen are reported in Figure 3 for the pristine PEGDA resin: it was evaluated 88% of acrylic double bond conversion. The presence of the precursor did not influence at all the final conversion (see data in Table 1), confirming the kinetic investigation data.

All the cured films showed a high gel content (>88%, see Table 1) indicating the absence of extractable oligomers or monomers, therefore confirming the conversion data, which show that the UV curing process was quite efficient in polymer network formation.

The DSC analyses showed that the silver nanoparticles did not influence significantly the $T_g$ behavior of the crosslinked polymer network. A rubbery polymer material was always obtained with a $T_g$ around 228–233 K (see Table 1).

The TGA analyses evidenced the presence of char content, which increased with increasing silver precursor content in the photocurable formulation (see Table 2). It is possible to attribute the char content to the silver formed during the photoreduction process. The char content is always very close to the theoretical silver amount, calculated on the basis of silver precursor content taking into account a complete reduction of the silver salt.

All the cured films were transparent which could probably indicate the absence of any macroscopic silver particle agglomeration. In Figure 4 the UV-vis spectrum of the cured films shows the presence of a strong absorption peak centered at around 450 nm, which is close to the reported surface plasmon resonance for silver NPs in solution.[13] The size and shape of metal NPs determine the spectral position of plasmon band absorption. It is evident from the spectra reported in Figure 4 that a slight shift of the maximum peak of the plasmon resonance toward longer wavelength occurred with increasing amount of silver precursor. This could be due to a larger aggregation phenomena, as a result of a higher number of silver NPs being present during the photoreduction process.

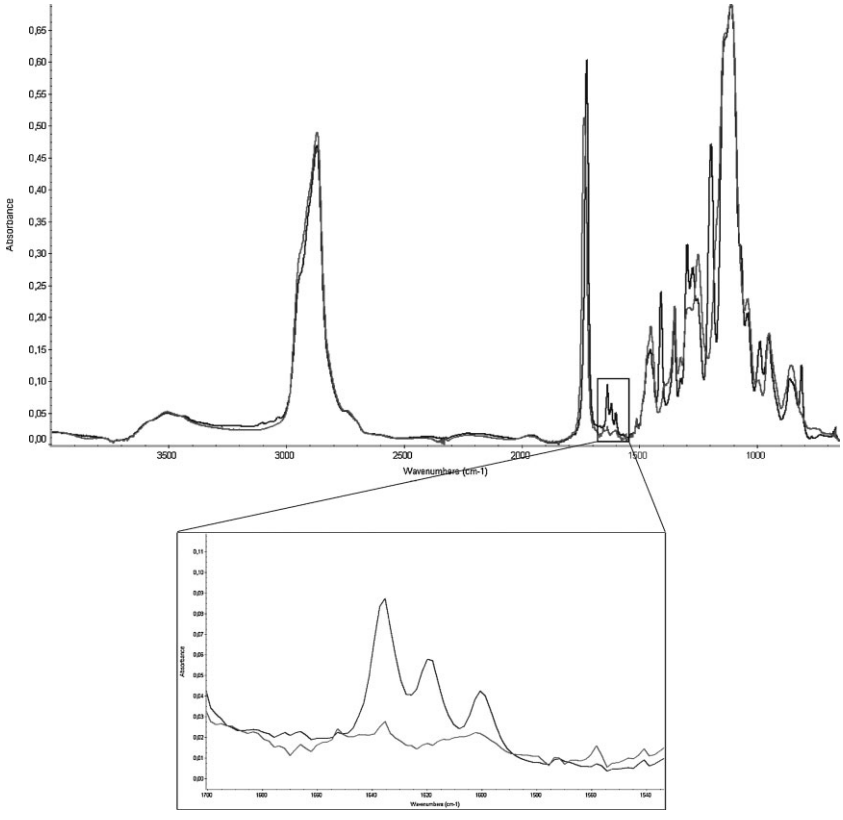


*Figure 3.* FT-IR spectra before and after 30 s curing in nitrogen atmosphere for the pristine PEGDA resin containing 2 wt.-% of radical photoinitiator.

## Morphology

An accurate morphology investigation of the cured films was performed by FESEM analyses and Matlab® image processing.

The silver particle equivalent diameter distributions extracted from the FESEM images, taken from freshly polymerized samples (indicated in Figure 6 "As polymerized") and the same materials sub-

*Table 1.* Properties of UV-cured PEGDA based films containing increasing content of silver precursor in range between 5 and 15 wt.-% with respect to the acrylic resin content.

| Sample[a)] | Conversion[b)] | Gel content[c)] | $T_g$[d)] |
|---|---|---|---|
| | % | % | K |
| PEGDA600 | 88 | 88 | 226 |
| PEGDA600 + 5 wt.-% $AgSbF_6$ | 90 | 88 | 227 |
| PEGDA600 + 10 wt.-% $AgSbF_6$ | 90 | 91 | 230 |
| PEGDA600 + 15 wt.-% $AgSbF_6$ | 89 | 93 | 230 |

[a)]Samples containing 2 wt.-% of radical photoinitiator cured under nitrogen; [b)]Determined by means of FT-IR by integrating the peak centered at 1 635 $cm^{-1}$ before and after 1 min of irradiation; [c)]Determined gravimetrically after 24 h extraction in chloroform, ASTM D2765-84; [d)]Measured by means of DSC.

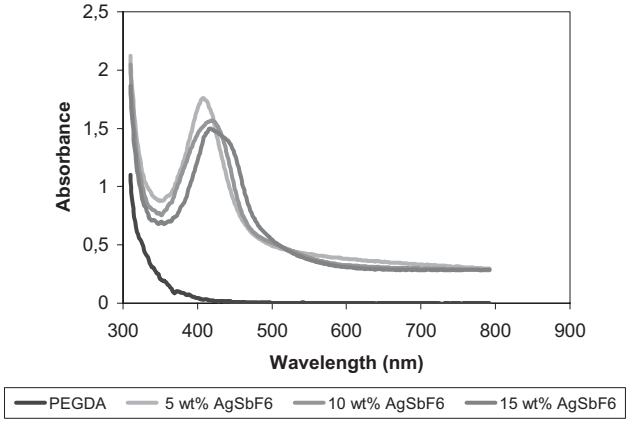


*Figure 4.* UV-vis absorbance spectra of UV-cured PEGDA based films containing increasing amount of silver precursor, providing evidence of silver surface plasmon resonance.

mitted to an electric stress (that we will refer to as electroaging/electroaged) show, interestingly, different shapes, as clearly indicated by the histograms of Figure 5. A single peak centered around 17 pixels (14 nm) appears in the former, while the latter shows a clear bifurcation of the particle population, having a peak around 10 and 27 pixels (7 and 21 nm respectively). Since the absolute value of recognized particles having a diameter bigger than 10 px (7 nm) was roughly the same for the two samples, the bifurcation of the distribution is consistent with electromigration and particle growth assisted from current flow, producing a lack of NPs with intermediate size (17 px, 14 nm) and a number of bigger particles. Looking into greater detail, the equivalent diameter, distance and eccentricity distributions of every sample in different storage conditions are shown in Figure 6. Note that freshly prepared samples featured a maximum equivalent diameter of the Ag NPs close to a concentration of 10 to 15%, while a more stable configuration obtained with simple aging of the samples resulted in a completely different distribution, with a maximum dimension of Ag NPs of around 20 nm localized at 5% of silver precursor. Samples with a very high amount of Ag, such as 40% of precursor, showed 15 nm particles – very far from the other results (out of scale; 120 nm median). This fact may explain the poor electrical properties found in this case, which will be described further in the following.

*Table 2.* Thermal stability and char content determined in UV-cured films by means of TGA analyses.

| Sample | $T_{10}$[a)] | $T_{50}$[b)] | Char content at 1 073 K | Theoretical char content |
|---|---|---|---|---|
| | K | K | % | % |
| PEGDA600 | 515 | 671 | 0.3 | 0 |
| PEGDA600 + 3 wt.-% $AgSbF_6$ | 509 | 675 | 1.8 | 0.9 |
| PEGDA600 + 5 wt.-% $AgSbF_6$ | 509 | 675 | 2.7 | 1.5 |
| PEGDA600 + 7 wt.-% $AgSbF_6$ | 476 | 672 | 3.1 | 2.1 |
| PEGDA600 + 10 wt.-% $AgSbF_6$ | 475 | 623 | 4.1 | 2.8 |
| PEGDA600 + 15 wt.-% $AgSbF_6$ | 477 | 630 | 5.0 | 4.0 |

[a)]$T_{10}$ is the temperature at which a weight loss of 10% of the sample is reached; [b)]$T_{50}$ is the temperature at which a weight loss of 50% of the sample is reached.

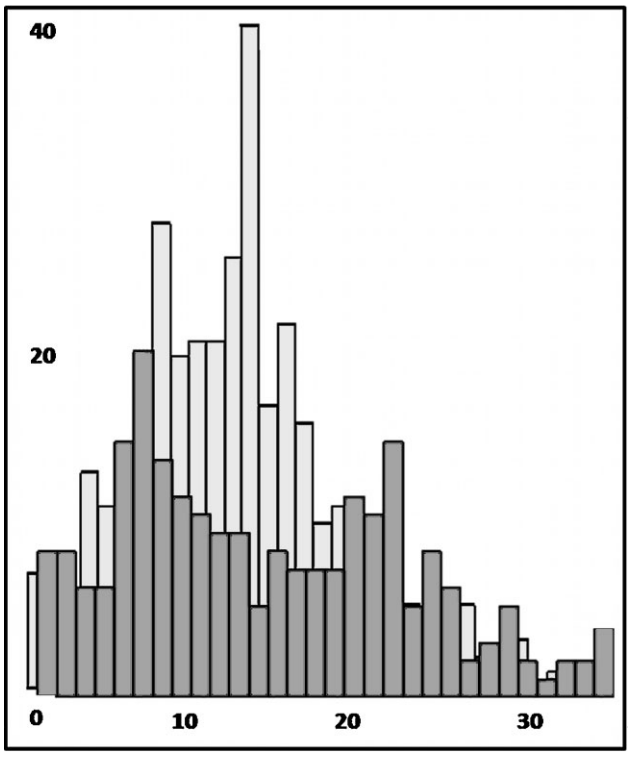


*Figure 5.* Equivalent diameter distributions for sample with 10% Ag, as polymerized (light gray, background) and after electroaging (dark gray, foreground). Indicated labels are expressed in nm.

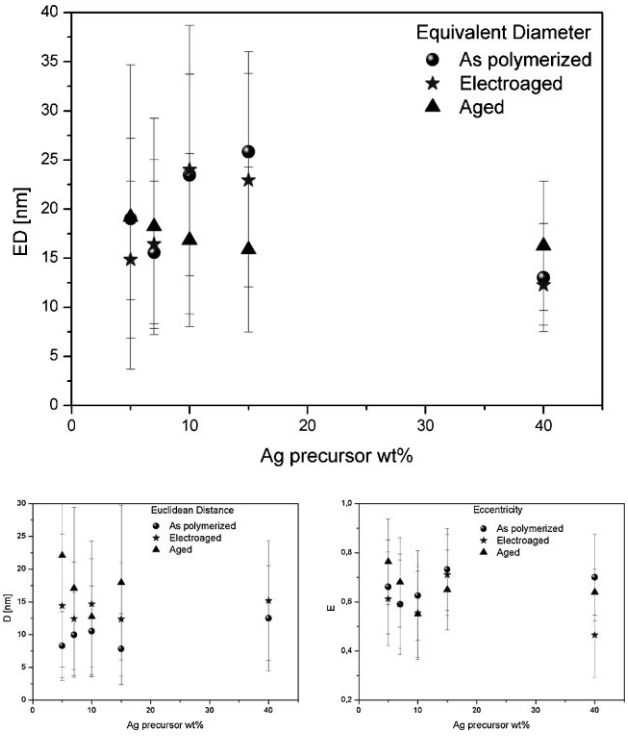


*Figure 6.* Equivalent diameter, distance and eccentricity distributions for cured PEGDA films containing increasing Ag precursor contents. The bars are used to indicate the standard deviation of the population, while full dots correspond to the median.

### Electrical Properties

The electrical properties of the samples are summarized in Figure 7 (top), where a number of different formulations (Ag precursor content from 0 to 40%) under different storage conditions were prepared. The resistivity, extracted from the simple *I/V* curve, is also shown. What is clear from the data cloud is that a resistivity minimum occurs around Ag precursor concentrations ranging from 7 to 10% and that the storage conditions (electroaged or simply aged) are very important for obtaining a stable electrical behavior. Globally the PEGDA samples showed a very linear Ohmic response over the explored domain, as shown in Figure 7 (bottom).

### Models Correlating Morphology with Electrical Properties

Trying to find a general law that allows the morphological features of the NP population to be correlated with the electrical properties, we propose a figure of merit (fom) depending on the number of NPs ($n$), the equivalent diameter (ED), the eccentricity ($E$), the branching factor (BF), the number of branched particles (BG) and the distance ($D$). All these parameters are correlated in Equation (1):

$$\text{fom} = \frac{n \times \text{ED} \times \text{BG}}{D \times E \times \text{BF}} \tag{1}$$

Where the quantities that affect positively the conductivity have been considered directly proportional to the fom and the ones affecting it negatively have been considered inversely proportional (also considering their range). The results are shown in Figure 8: plotted in bi-logarithmic coordinates, the behavior of the PEGDA system is pretty linear, providing that for samples with 0% Ag precursor is assigned a fom $< 1$. Different storage conditions result in quite different data clouds. It is very important to consider every aspect of the particle size, distribution, branching and eccentricity. Another possible visualization scheme is that of Figure 9: here a three-dimensional plot was generated, whose *XYZ* coordinate system includes the resistivity, the morphological figure of merit and the Ag content. The optimal conditions for low resistivity are indicated by the top-right portion of the transparent surface superimposed on the data. Nevertheless, the most conductive samples featured similar values of fom, suggesting that this model is not adequate to describe

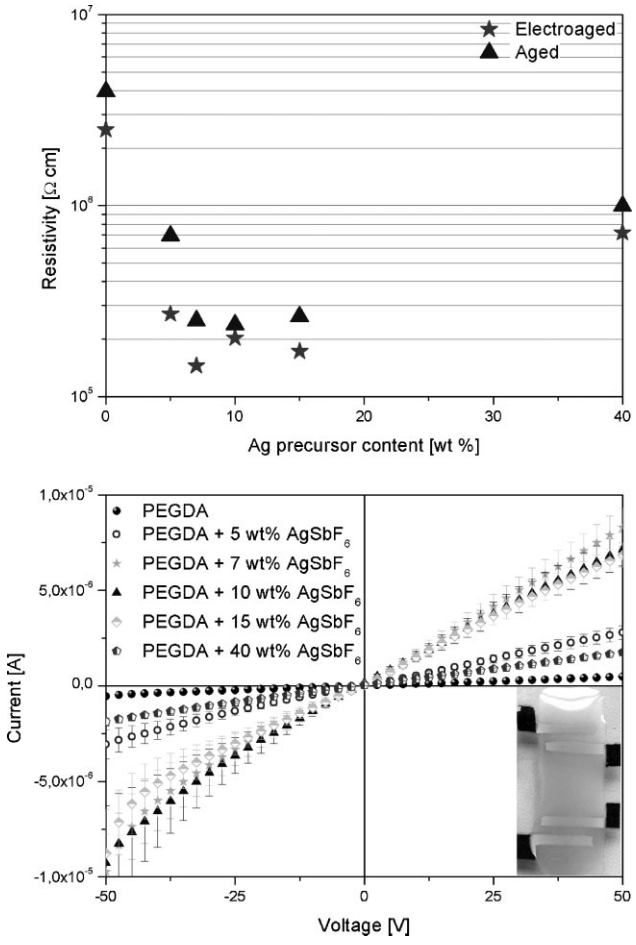


*Figure 7.* Resistivity versus Ag precursor content for different batches where the storage conditions have been varied. Top: phase plot; bottom: *I/V* curves; inset: geometry of the sample for electrical characterization (outer electrodes for the current injection, inner electrodes for the voltage drop reading).

our nanocomposite in detail. For this reason, we explored two models to reproduce the characteristic shape of Figure 7: the first is adapted from the percolation theory, the second from the extended Vegard law used to describe the properties of binary compounds.

Percolation theory[6,14] is a universal model able to describe the properties of disordered systems. The polymeric composite was modeled as a dissipative lattice where $p$ sites are occupied by conductive Ag nodes in a dissipative PEGDA matrix; when a particular state, criticality, is reached, percolation occurs and the electrical conductivity of the system undergoes a discontinuity. The critical concentration only depends on the lattice properties; we used two models to fit experimental data, the cubic three-dimensional lattice characterized by $d = 3$, $z = 6$ ($d$ spatial dimensions and $z$ coordination number) and $d = 2$, $z = 3$, namely a square hexagonal lattice. For these models, we have a criticality before percolation at $p_c = 0.6962$ and

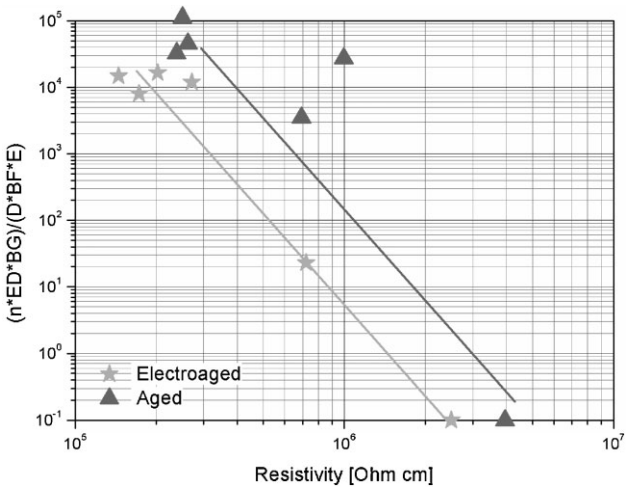


*Figure 8.* Resistivity correlation between morphological and electrical properties for the cured films containing Ag NPs. Correlation based on the parameters collected according to Equation (1). The lines are a guide for the eye.

0.3116, respectively.[6] The FESEM planar images that correspond to the real lattice should be classified with $2 < d < 3$ and $3 < z < 6$, since the signal coming from the NPs is not limited to a flat surface but comes from a slab up to 2 μm thick. The occupation probability is written in terms of image statistical properties:

$$p = \frac{\sum_{i=1}^{n} \pi a_i b_i}{MN} \tag{2}$$

where $M$ and $N$ are the FESEM image size (each pixel is treated as a lattice point) and the quantity at numerator is

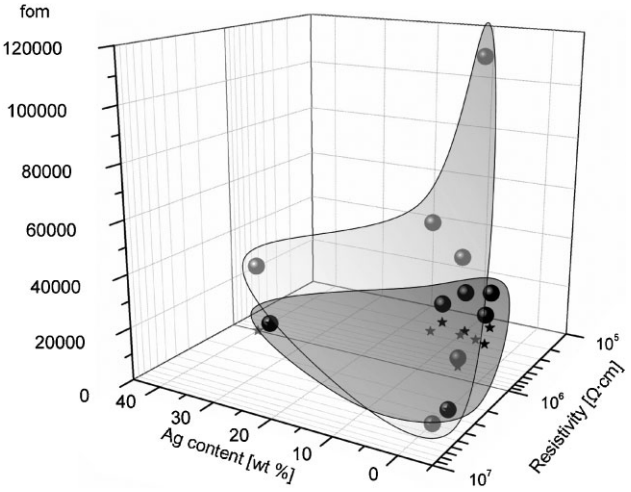


*Figure 9.* Three-dimensional phase plot for PEGDA resin with Ag NPs. The transparent surfaces indicates the existence condition for analyzed samples, the more favorable conditions for low resistivity being in the topmost right portion of the surfaces.

*Table 3.* Occupation probabilities based on the FESEM image of a fracture section; sites computed according to Equation (2).

| Sample | Occupation probability | | |
|---|---|---|---|
| | As polymerized | Electroaged | Aged |
| PEGDA600 + 5 wt.-% $AgSbF_6$ | 0.200 | 0.107 | 0.119 |
| PEGDA600 + 7 wt.-% $AgSbF_6$ | 0.160 | 0.140 | 0.118 |
| PEGDA600 + 10 wt.-% $AgSbF_6$ | 0.219 | 0.195 | 0.136 |
| PEGDA600 + 15 wt.-% $AgSbF_6$ | 0.301 | 0.187 | 0.090 |
| PEGDA600 + 40 wt.-% $AgSbF_6$ | 0.095 | 0.066 | 0.004 |

the sum of all the areas of the NPs, *a* and *b* being their axes (in pixel). In other terms, *p* is the ratio of the white pixels over the sum of white and black ones. The criticality value, computed according to Equation (2) and reported in Table 3, was far from being reached for all the samples. The steady state resistivity was found to increase with occupation probability (Ag precursor content) with a power law, whose exponent is universal:

$$\rho = (p_c - p)^s \tag{3}$$

where s = *1.30* for the two-dimensional lattice and s = *0.74* for the three-dimensional one.[6] Equation (3) was used to fit experimental data, as shown in Figure 10; so obtained curves of resistivity versus Ag precursor content present a characteristic minimum feature, placed at low concentrations (around 7% to 10% of the precursor), that qualitatively mimic the experimental behavior. Nevertheless neither the cubic nor the hexagonal lattice of conductive elements in a dissipative matrix realized a good fit.

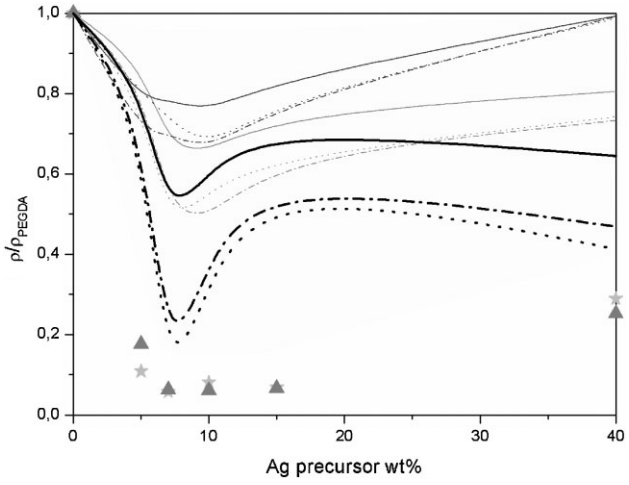


*Figure 10.* Statistical and geometrical models for resistivity versus Ag content. Tones: light grey refers to the aged sample, thick black to the electroaged one, dark gray to the as polymerized one. Dots: experimental values; full line: three-dimensional cubic lattice, Equation (3); dotted line: two-dimensional hexagonal lattice, Equation (3); dot-dash: geometrical model based on Equation (5).

Another approach was applied, using the extended Vegard law,[15] here adapted to model the resistivity in a binary system formed by a PEGDA matrix and a certain number of Ag aggregates:

$$\rho \approx (1 - p)\rho_{PEGDA} + p\rho_{Ag} \tag{4}$$

By substituting the former Equation (2) and considering that, to a first approximation, the sum of all NP areas may be substituted by the mean area times the number of NPs, one has:

$$\rho \approx (1 - \pi n\langle a\rangle\langle b\rangle)\rho_{PEGDA} + \pi n\langle a\rangle\langle b\rangle\rho_{Ag} \tag{5}$$

where the mean NP axes are correlated to the extracted image features *E* and ED by the following system of equations:

$$\begin{aligned}\langle a\rangle &= \sqrt{\frac{\langle ED\rangle}{\sqrt{1 - \langle E\rangle^2}}} \\ \langle b\rangle &= \sqrt{\langle ED\rangle\sqrt{1 - \langle E\rangle^2}}\end{aligned} \tag{6}$$

This model behaved better than the statistical ones, as shown in Figure 10 (dot-dash lines), probably because it describes in a better detail the sample geometry. Interestingly, models (3) and (5) may be applied also to the as polymerized sample, whose "geometrical" resistivity is very close to the order of magnitude of measured samples (dark gray lines). The authors suggest that probably other conduction mechanisms have to be considered in the physical models to be effective, for example interfacial conduction (over the NP surface) that may further reduce resistivity below percolation threshold, as reported for different systems such as ionic conductors.[16]

## Conclusion

Conductive UV-curable acrylic inks were prepared via bottom-up approach in which silver NPs were generated

in situ: a simultaneous photoinduced electron transfer and radical polymerization process occurred in the presence of a radical photoinitiator, under UV light. The silver precursor did not influence the photopolymerization process which occurred with high acrylic double bond conversion (around 90%), giving rise to UV-cured films with high gel content (always above 88%).

An accurate morphological characterization was performed on UV-cured films through FESEM analyses and Matlab image processing: this allowed the correlation between morphology and electrical properties to be reported for the cured polymers, which were characterized at room temperature. In order to explain the resistivity versus Ag precursor content, we developed a specific figure of merit and tested two models: the universal percolation theory for both a two-dimensional hexagonal and a three-dimensional cubic lattice and a modified version of the Vegard law for composites. A general inefficacy of the models to predict the resistivity of the cured samples as a function of the Ag precursor content casts some light on the nature of the conduction mechanism of this material. The authors suggest that those mechanisms could be heavily influenced by superficial conduction phenomena on the edge of dispersed Ag NPs.

Acknowledgements: The authors would like to thank the *Regione Piemonte* that funded this research within the *PrintTAG Project* ("Sistemi Avanzati di Produzione", 2008).

Received: May 4, 2010; Revised: June 22, 2010; Published online: August 16, 2010; DOI: 10.1002/macp.201000242

Keywords: conducting polymers; nanoparticles; photochemistry; silver; structure/property relationships

[1] Q. D. Ling, D. J. Liaw, C. Zhu, D. S. H. Chan, E. T. Kang, K. G. Neoh, *Prog. Polym. Sci.* **2008**, *33*, 917.
[2] H. Sirringhaus, N. Tessler, R. H. Friend, *Science* **1998**, *280*, 1741.
[3] Y. Wattanabe, K. Kuda, *Appl. Phys. Lett.* **2005**, *87*, 2235.
[4] T. W. Kelley, C. D. Frisbie, *J. Phys. Chem. B* **2001**, *105*, 4538.
[5] B. K. Krone, A. Dodabalapur, R. Sarpeshkar, A. Gelperin, H. E. Katz, Z. Bao, *J. Appl. Phys.* **2002**, *91*, 10140.
[6] H. Bunde, S. Havlin, *Fractals and disordered systems*, Springer Verlag, Heidelberg 1996.
[7] M. Sangermano, Y. Yagci, G. Rizza, *Macromolecules* **2007**, *40*, 8827.
[8] Y. Yagci, M. Sangermano, G. Rizza, *Polymer* **2008**, *49*, 5159.
[9] Y. Yagci, M. Sangermano, G. Rizza, *Chem. Commun.* **2008**, *24*, 2771.
[10] Y. Yagci, M. Sangermano, G. Rizza, *Macromolecules* **2008**, *41*, 7268.
[11] J. P. Fouassier, J. C. Rabek, *Radiation Curing in Polymer Science and Technology*, Vol. I, Elsevier, London 1993.
[12] M. Sangermano, R. Bongiovanni, G. Malucelli, A. Priola, in: *Horizons in Polymer Research*, R. K. Bregg, Ed. Nova Science Publishers, New York 2006, pp. 61–82.
[13] S. L. Smitha, K. M. Nissamudeen, D. Philip, K. G. Gopchandran, *Spectrochim. Acta* **2008**, *71*, 186.
[14] M. Sahimi, *Application of percolation theory*, Taylor & Francis, London 1994.
[15] L. Vegard, *Zeitsch. Phys.* **1921**, 5.
[16] F. W. Poulsen, N. H. Andersen, B. Kinde, J. Schoonman, *Solid State Ionics* **1983**, *9/10*, 119.